Acta Crystallographica Section F
Structural Biology and Crystallization Communications
ISSN 1744-3091

Noncanonical conformation of CDR L1 in the anti-IL-23 antibody CNTO4088

Alexey Teplyakov,* Galina Obmolova, Alison Rogers and Gary L. Gilliland

Centocor R&D Inc., 145 King of Prussia Road, Radnor, PA 19087, USA

Correspondence e-mail: ateplyak@its.jnj.com

Received 13 November 2009
Accepted 15 December 2009

PDB Reference: CNTO4088, 3i2c.

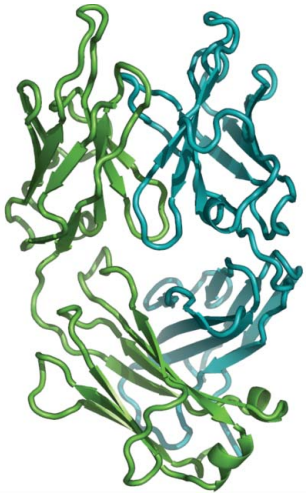

CNTO4088 is a monoclonal antibody to human IL-23. The X-ray structure of the Fab fragment revealed an unusual noncanonical conformation of CDR L1. Most antibodies with the κ light chain exhibit a canonical structure for CDR L1 in which residue 29 anchors the CDR loop to the framework. Analysis of the residues believed to define the conformation of CDR L1 did not explain why it should not adopt a canonical conformation in this antibody. This makes CNTO4088 a benchmark case for developing prediction methods and structure-modeling tools.

1. Introduction

CNTO4088 is a monoclonal antibody (mAb) to human interleukin-23 (IL-23), a heterodimeric cytokine consisting of two subunits: p40 and p19. The p40 subunit can also associate with a separate protein subunit, p35, to form another cytokine, IL-12. Both IL-23 and IL-12 can activate the transcription activator STAT4 and stimulate the production of interferon-γ (Oppmann *et al.*, 2000). However, the receptor binding of the unique subunit (p19 for IL-23 and p35 for IL-12) confers cytokine-specific intracellular signaling. The biological functions of IL-23 are distinct from those of IL-12, despite the structural similarity between the two cytokines. IL-23 is an important part of the inflammatory response against infection. It promotes upregulation of the matrix metalloprotease MMP9, increases angiogenesis and reduces CD8+ T-cell infiltration (Kastelein *et al.*, 2007). In conjunction with IL-6 and TGF-β1, IL-23 stimulates the differentiation of naive CD4+ T-cells that leads to production of a proinflammatory cytokine IL-17 (Aggarwal *et al.*, 2003; Yen *et al.*, 2006).

Abnormal regulation of IL-23 and IL-12 has been associated with many immune-mediated diseases since their neutralization by antibodies is effective in treating animal models of psoriasis, multiple sclerosis, rheumatoid arthritis, inflammatory bowel disease, insulin-dependent (type 1) diabetes mellitus and uveitis (Davidson *et al.*, 1998; Hong *et al.*, 1999; Leonard *et al.*, 1995; Malfait *et al.*, 1998). Neutralization of IL-23 without inhibition of IL-12 pathways can provide effective therapy of immune-mediated diseases with limited impact on important host defense immune mechanisms.

CNTO4088 was generated through immunization of mice (manuscript in preparation). It is specific to IL-23 and does not bind IL-12. The crystal structure of the CNTO4088 Fab was determined at 2.8 Å resolution. CNTO4088 exhibits an unusual conformation of CDR L1 which cannot be inferred from sequence analysis.

2. Experimental methods

2.1. Antibody cleavage and Fab purification

For Fab generation, 50 mg CNTO4088 mAb (mouse IgG1κ) was dialyzed into buffer containing 20 m*M* sodium phosphate pH 7.0 and 10 m*M* EDTA and diluted to 10 mg ml^{-1}. Antibody digestion was performed using the ImmunoPure Fab Preparation Kit (Pierce,

Table 1
Crystallographic statistics.

Values in parentheses are for the highest resolution shell.

Data collection	
Resolution (Å)	50–2.8 (2.9–2.8)
Reflections measured	97048 (10138)
Unique reflections	13889 (1547)
Completeness (%)	99.9 (100)
Redundancy	6.9 (6.6)
R_{merge}†	0.169 (0.449)
$\langle I/\sigma(I)\rangle$	6.0 (2.0)
B factor (Wilson plot) (Å^2)	87.2
Refinement	
Resolution (Å)	15–2.8
Reflections used in refinement	12686
No. of atoms	3359
No. of water molecules	2
R factor‡	0.196
R_{free}‡ (7.5% of data)	0.235
R.m.s. deviations	
Bond lengths (Å)	0.008
Bond angles (°)	1.3
Mean B factor (Å^2)	58.9
Ramachandran plot	
Most favored region (%)	84.4
Additionally allowed region (%)	14.0
Generously allowed region (%)	1.3
Disallowed region (%)	0.3

† $R_{merge} = \sum_{hkl}\sum_i |I_i(hkl) - \langle I(hkl)\rangle| / \sum_{hkl}\sum_i I_i(hkl)$, where $I_i(hkl)$ is the intensity of the ith observation of unique reflection hkl and $\langle I(hkl)\rangle$ is the average intensity. ‡ $R = \sum_{hkl} ||F_{obs}| - |F_{calc}|| / \sum_{hkl} |F_{obs}|$, where F_o are the observed and F_c are the calculated structure factors.

Rockford, Illinois, USA) according to the manufacturer's instructions. Immobilized papain (5 ml, suspended) was incubated with CNTO4088 mAb (5 ml at 10 mg ml^{-1}) for 8 h in a shaker at 310 K. The digested protein was separated from the resin using serum separators (Pierce, Rockford, Illinois, USA) and was incubated overnight at 277 K with 8 ml Protein G resin (GE Healthcare, Piscataway, New Jersey, USA) to separate the Fab from the other proteins.

The Fab was further purified using a 1 ml HiTrap Protein A FF column (GE Healthcare, Piscataway, New Jersey, USA). The sample was loaded at 0.5 ml min^{-1}. The Fab-containing fractions were pooled, concentrated and run over a Superdex 75 10/300 GL column (GE Healthcare, Piscataway, New Jersey. USA) in 1× PBS buffer at 0.5 ml min^{-1}. Fractions of 0.2 ml were collected and analyzed by SDS–PAGE and size-exclusion HPLC. The Fab-containing fractions were pooled and dialyzed into 20 m*M* Tris pH 7.5, 10 m*M* NaCl. The final purification step was performed on a MonoQ 5/50 column (GE Healthcare, Piscataway, New Jersey, USA) equilibrated with 20 m*M* CHES pH 9.5 and 10% glycerol. The protein was eluted with a linear gradient of 0–100 m*M* NaCl and was concentrated to 4.5 mg ml^{-1}. The final yield of the Fab was about 5 mg.

2.2. Crystallization

Crystallization of CNTO4088 Fab was carried out by the hanging-drop vapor-diffusion method at 293 K. The experiments were composed of droplets of 0.8 µl 4.5 mg ml^{-1} protein solution in 20 m*M* Tris pH 7.5, 10 m*M* NaCl, 10% glycerol mixed with 0.8 µl reservoir solution. The droplets were equilibrated against 1 ml reservoir solution. Initial screening was performed with Crystal Screen I and II (Hampton Research, Aliso Viejo, California, USA), and Wizard I and II (Emerald BioSystems, Bainbridge Island, Washington, USA) crystallization screens. An optimized screening yielded well shaped crystals from 24% PEG 8000, 0.1 *M* citrate buffer pH 3.5. X-ray diffraction-quality crystals were grown over two months using the seeding technique. They belonged to the tetragonal space group *I*4, with unit-cell parameters $a = b = 99.43$, $c = 115.04$ Å. The asymmetric part of the unit cell contained one Fab molecule, which corresponds to a V_M of 3.0 Å^3 Da^{-1}. The solvent content of the crystals was 59%.

2.3. X-ray data collection and structure determination

For X-ray data collection, one crystal was soaked for a few seconds in a cryoprotectant solution containing 24% PEG 8000, 0.1 *M* citrate pH 3.5 and 15% ethylene glycol and flash-frozen in a stream of nitrogen at 100 K. X-ray diffraction data were collected using a Rigaku MicroMax-007HF microfocus X-ray generator equipped with Osmic VariMax confocal optics, a Saturn 944 CCD detector and an X-stream 2000 cryocooling system (Rigaku, The Woodlands, Texas, USA). Diffraction intensities were detected over 180° of crystal rotation with an exposure time of 120 s per 0.5° image. The X-ray data were processed with the program *d*TREK* (Rigaku, The Woodlands, Texas, USA). The diffraction pattern indicated a deviation from a single lattice; many reflections appeared to be split owing to a likely crystal fracture. Depending on the crystal orientation, the effect varied in magnitude. This certainly had an impact on the R_{merge} values, particularly at low resolution, where they are in the range 6–10%, leading to an overall R_{merge} of 16.9% (Table 1). However, the quality of the data was sufficiently high, as evidenced by the unambiguous molecular-replacement solution and by the refinement results (see below).

The structure was determined by molecular replacement using *AMoRe* (Navaza, 1994). The crystal structure of the influenza hemagglutinin antibody BH151 Fab (PDB entry 1eo8; Fleury *et al.*, 2000) was used as a search model. Atomic positions and temperature

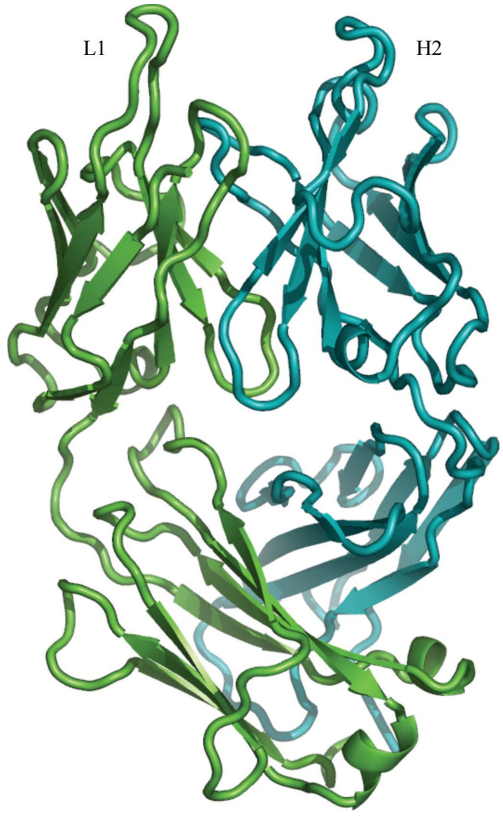

Figure 1
Ribbon representation of CNTO4088 Fab (light chain, green; heavy chain, blue). Long CDR loops are labeled.

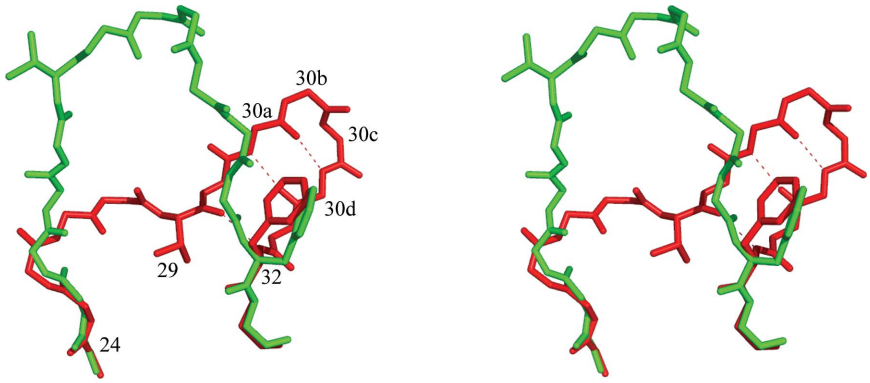

Figure 2
Superposition of CDR L1 in 1f58 (canonical conformation; red) and CNTO4088 (green). Side chains are only shown for Val29 and Phe32. Residues are numbered according to Chothia & Lesk (1987). Hydrogen bonds in 1f58 are shown as dashed lines.

factors were refined with *REFMAC* (Murshudov *et al.*, 1997) with tightly restrained geometry using all reflections in the resolution range 15–2.8 Å. The refinement statistics are given in Table 1. All crystallographic calculations were performed using the *CCP*4 suite of programs (Collaborative Computational Project, Number 4, 1994). Model adjustments were carried out using *Coot* (Emsley & Cowtan, 2004). Residues are numbered according to the scheme of Chothia & Lesk (1987). The atomic coordinates and structure factors have been deposited in the Protein Data Bank under code 3i2c.

3. Results and discussion

The structure of CNTO4088 Fab contained all residues up to the C-terminal interchain disulfide, which was disordered. Seven proline residues were observed in *cis* conformations, four in the light chain (Pro8, Pro81, Pro99 and Pro145) and three in the heavy chain (Pro154, Pro156 and Pro196), which is typical for the IgG1κ antibody. One residue, Ala51 in the light chain, falls into a disallowed region of the Ramachandran plot. The main-chain conformation of Ala51 ($\varphi = 67^\circ$, $\psi = -49^\circ$) is often observed for the residue in the β-turn of the second antigen-binding loop.

The antigen-binding site is composed of six complementarity-determining regions (CDRs) labeled L1, L2 and L3 in the light chain and H1, H2 and H3 in the heavy chain (Wu & Kabat, 1970). CNTO4088 has relatively long L1 and H2 CDRs and short L3 and H3 CDRs. This creates an antigen-binding surface with a deep crevice in the middle surrounded by the long loops L1 and H2 (Fig. 1). The short loops L3 and H3 form the bottom of the putative binding site. The amino-acid distribution shows a high proportion of charged residues and almost no hydrophobic residues, suggesting that polar interactions rather than hydrophobic interactions may play a role in the antibody–antigen recognition.

Five of the six CDR loops (with the exception being H3) have been shown to adopt a small number of main-chain conformations called canonical structures (Chothia & Lesk, 1987). CDR H3 appears to adopt too many conformations to be classified. The conformation of a particular canonical structure is determined by the length of the loop and the residues in key positions. Assignment of canonical structures for CNTO4088 was carried out with the help of Andrew Martin's resource at http://www.bioinf.org.uk/abs (Abhinandan & Martin, 2008). CDRs H1, H2, L2 and L3 belong to the most populated classes observed in many other antibodies, namely to classes 10A, 12B, 7A and 9A, respectively (the number in the class name corresponds to the CDR length).

CDR L1 contains 15 residues, with those at the insertion site labeled according to the convention of Chothia & Lesk (1987) as 30a, 30b, 30c and 30d. CDR L1 forms a wide loop that cannot be assigned to any existing canonical class (Fig. 2). The loop makes very few contacts with other CDRs and only one crystal contact, which is made through the side chain of Tyr30d. These contacts do not appear to be

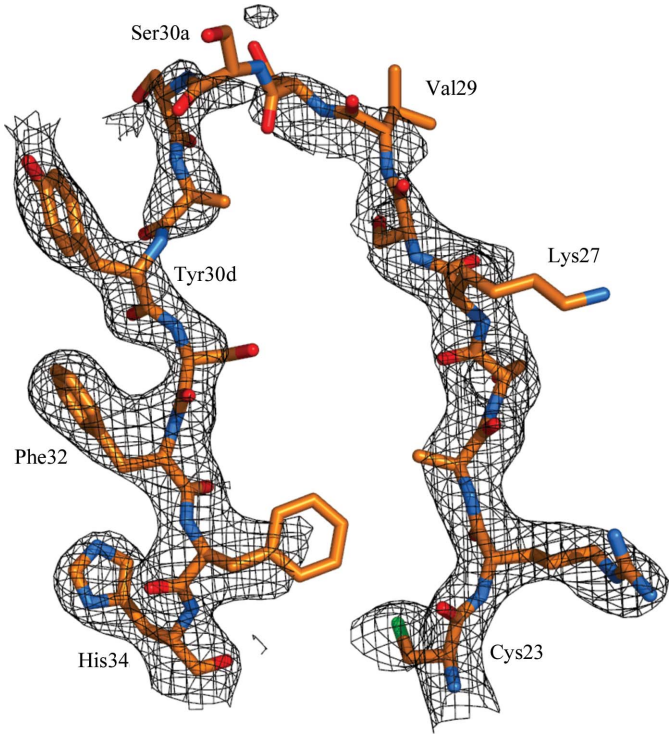

Figure 3
Electron density for CDR L1 in CNTO4088 Fab (OMIT $2F_o - F_c$ map contoured at the 1.5σ level).

```
          2..24              34..71
3i2c    I...RASKSVSSSAYSFFH...F
1i7z    L...RASKSVSTSGYNYMH...F
1i9r    I...RASQRVSSSTYSYMH...F
1ibg    I...RASKSVSTSGYSHIH...F
3dgg    I...RASKSVSTSGYSYMH...F
1f58    I...KASQGVDFDGASFMN...F
```

Figure 4
Residues in positions 2, 24–34 (CDR L1) and 71 of the light chain. PDB entry 3i2c is the present structure (CNTO4088).

strong or numerous enough to account for the unusual conformation of CDR L1. Although the electron density is weak for some side chains, the tracing of the backbone is unambiguous (Fig. 3).

A number of residues in CDR L1 as well as those in positions 2, 25, 33 and 71, which are involved in the packing of the CDR against the framework, have been identified as determining the conformation of the loop (Chothia & Lesk, 1987; Tramontano *et al.*, 1990; Martin & Thornton, 1996). It appears that the key residues in CNTO4088 are very similar to those of other antibodies [PDB entries 1ibg (Jeffrey *et al.*, 1995), 1f58 (Stanfield *et al.*, 1999), 1i7z (Larsen *et al.*, 2001), 1i9r (Karpusas *et al.*, 2001) and 3dgg (Nettleship *et al.*, 2008)], all of which adopt the canonical structure (Fig. 4). Therefore, it is hard to rationalize why CNTO4088 adopts a noncanonical structure. As a rare exception, the structure of CNTO4088 may contribute to a better understanding of sequence–structure relationships in antibodies.

References

Abhinandan, K. R. & Martin, A. C. R. (2008). *Mol. Immunol.* **45**, 3832–3839.
Aggarwal, S., Ghilardi, N., Xie, M. H., de Sauvage, F. J. & Gurney, A. L. (2003). *J. Biol. Chem.* **278**, 1910–1914.
Chothia, C. & Lesk, A. M. (1987). *J. Mol. Biol.* **196**, 901–917.
Collaborative Computational Project, Number 4 (1994). *Acta Cryst.* D**50**, 760–763.
Davidson, N. J., Hudak, S. A., Lesley, R. E., Menon, S., Leach, M. W. & Rennick, D. M. (1998). *J. Immunol.* **161**, 3143–3149.
Emsley, P. & Cowtan, K. (2004). *Acta Cryst.* D**60**, 2126–2132.
Fleury, D., Daniels, R. S., Skehel, J. J., Knossow, M. & Bizebard, T. (2000). *Proteins*, **40**, 572–578.
Hong, K., Chu, A., Ludviksson, B. R., Berg, E. L. & Ehrhardt, R. O. (1999). *J. Immunol.* **162**, 7480–7491.
Jeffrey, P. D., Schildbach, J. F., Chang, C. Y., Kussie, P. H., Margolies, M. N. & Sheriff, S. (1995). *J. Mol. Biol.* **248**, 344–360.
Karpusas, M., Lucci, J., Ferrant, J., Benjamin, C., Taylor, F. R., Strauch, K., Garber, E. & Hsu, Y.-M. (2001). *Structure*, **9**, 321–329.
Kastelein, R. A., Hunter, C. A. & Cua, D. J. (2007). *Annu. Rev. Immunol.* **25**, 221–242.
Larsen, N. A., Zhou, B., Heine, A., Wirsching, P., Janda, K. D. & Wilson, I. A. (2001). *J. Mol. Biol.* **311**, 9–15.
Leonard, J. P., Waldburger, K. E. & Goldman, S. J. (1995). *J. Exp. Med.* **181**, 381–386.
Malfait, A. M., Butler, D. M., Presky, D. H., Maini, R. N., Brennan, F. M. & Feldmann, M. (1998). *Clin. Exp. Immunol.* **111**, 377–383.
Martin, A. C. & Thornton, J. M. (1996). *J. Mol. Biol.* **263**, 800–815.
Murshudov, G. N., Vagin, A. A. & Dodson, E. J. (1997). *Acta Cryst.* D**53**, 240–255.
Navaza, J. (1994). *Acta Cryst.* A**50**, 157–163.
Nettleship, J. E., Ren, J., Rahman, N., Berrow, N. S., Hatherley, D., Barclay, A. N. & Owens, R. J. (2008). *Protein Expr. Purif.* **62**, 83–89.
Oppmann, B. *et al.* (2000). *Immunity*, **13**, 715–725.
Stanfield, R., Cabezas, E., Satterthwait, A., Stura, E., Profy, A. & Wilson, I. (1999). *Structure*, **7**, 131–142.
Tramontano, A., Chothia, C. & Lesk, A. M. (1990). *J. Mol. Biol.* **215**, 175–182.
Wu, T. T. & Kabat, E. A. (1970). *J. Exp. Med.* **132**, 211–250.
Yen, D., Cheung, J., Scheerens, H., Poulet, F., McClanahan, T., McKenzie, B., Kleinschek, M. A., Owyang, A., Mattson, J., Blumenschein, W., Murphy, E., Sathe, M., Cua, D. J., Kastelein, R. A. & Rennick, D. (2006). *J. Clin. Invest.* **116**, 1310–1316.